AIP Journal of Applied Physics

Bond-order potential for point and extended defect simulations in tungsten

T. Ahlgren, K. Heinola, N. Juslin, and A. Kuronen

Citation: Journal of Applied Physics **107**, 033516 (2010); doi: 10.1063/1.3298466
View online: http://dx.doi.org/10.1063/1.3298466
View Table of Contents: http://scitation.aip.org/content/aip/journal/jap/107/3?ver=pdfcov
Published by the AIP Publishing

Bond-order potential for point and extended defect simulations in tungsten

T. Ahlgren,[a] K. Heinola, N. Juslin, and A. Kuronen
Accelerator Laboratory, University of Helsinki, P.O. Box 43, Helsinki 00014, Finland

(Received 5 October 2009; accepted 3 January 2010; published online 8 February 2010)

A reactive interatomic bond-order potential for bcc tungsten is presented. Special attention in the potential development was given for obtaining accurate formation and migration energies for point defects, making the potential useful in atomic scale simulations of point and extended defects. The potential was used to calculate binding energies and trapping distances for vacancies in vacancy clusters and the recombination radius for self-interstitial atom and monovacancy. © *2010 American Institute of Physics*. [doi:10.1063/1.3298466]

I. INTRODUCTION

Tungsten (W), or also known as wolfram, is a group 6B transition metal with extraordinary physical and thermal properties. It has the lowest coefficient of thermal expansion and the highest melting point (3680 K) of any pure metal. Due to its refractory properties of retaining strength at high temperatures, W is used as filaments and electrodes in lamps, in gas tungsten arc welding and as the compound tungsten carbide in machining and cutting tools. The most spectacular application of tungsten is its intended use in the ITER fusion reactor.[1,2]

The mechanical and thermal properties of a material are ordinarily controlled by extended defects,[3] which in turn depend on the kinetics and energetics of point defects. The number and kind of point and extended defects are determined by the manufacturing process of the material, but can also be introduced by annealing, quenching, or irradiation. An excellent method for indirectly studying the basic recovery mechanisms of ion irradiated material is the resistivity measurement combined with isochronal annealing. This experimental method reveals the temperatures at which the material recovers after ion, electron, or neutron bombardment.[4,5] However, to identify these recovery stages which depend on the mobility, recombination, clustering, and dissociation of defects, the experimental data has to be compared with atomistic simulations, which rely on an accurate description of atomic interactions. Methods based on density functional theory (DFT) are the most reliable computational techniques for studying the physical and mechanical properties of materials.[6] However, due to the demanding need for computational power, the DFT calculations are limited to small size systems, e.g., point defect energetics. Studies of large and complex systems or time related processes using DFT calculations are at the present moment computationally not feasible. Simulations of large systems need computationally efficient description of the atomic scale interactions.

Realistic analytical potentials describing variations of the local chemical environment are nowadays available for a number of different materials. Central-force many-body potentials that describe well metallic materials are the embedded-atom method (EAM)[7,8] and Finnis–Sinclair (FS) type potentials.[9] Examples of schemes including noncentral forces are the modified embedded-atom method[10] and different tight-binding techniques.[11] An application of the fourth moment approximation of the tight-binding scheme for modeling tungsten surfaces was presented by Xu and Adams.[12] Analytical potentials to describe W has been developed by Derlet *et al.*[13] which cannot deal with high-energy collision dynamics, and by Juslin *et al.*[14] which gives too low point defect formation energies and wrong self-interstitial atom configuration.

The purpose of the present work is to obtain the set of parameters for a Tersoff–Brenner-type potential[15–17] with a well established functional form,[14,18] which besides bulk properties, also provides accurate formation and migration energies for point defects in W. Moreover, the potential can also be used for simulations involving high-energy collisions. In this work we apply the obtained bond-order potential (BOP) parameters set to find the configuration, trapping radius, and binding energies for W vacancy clusters and the recombination radius for self-interstitial atom and monovacancy.

II. BOND-ORDER FORMALISM AND PARAMETERS

Bond-order potentials are semiempirical schemes to calculate atomic interaction energies from the local arrangement of atoms. The functional form of the used bond-order potential has been discussed in details previously.[14,18,19] The total energy is a sum over individual bond energies

$$E = \sum_{i>j} f_{ij}^{c}(r_{ij})[V_{ij}^{\mathrm{R}}(r_{ij}) - b_{ij}V_{ij}^{\mathrm{A}}(r_{ij})], \tag{1}$$

where the pairlike repulsive and attractive terms are taken as Morse-like pair potentials

$$V^{\mathrm{R}}(r) = \frac{D_0}{S-1}\exp[-\beta\sqrt{2S}(r-r_0)], \tag{2}$$

$$V^{\mathrm{A}}(r) = \frac{SD_0}{S-1}\exp[-\beta\sqrt{2/S}(r-r_0)], \tag{3}$$

where the dimer bond energy D_0 and bond distance r_0 and the parameters S and β are all fitting parameters. The interaction is restricted by a cutoff-function

[a]Electronic mail: tommy.ahlgren@helsinki.fi.

TABLE I. Parameters for the W-W interaction developed in this work.

Parameter	Value
D_0 (eV)	3.282 547
r_0 (Å)	2.460 687
β (Å^{-1})	1.373 146
S	2.215 376
γ	0.001 293 884
c	1.327 324
d	0.135096
h	−0.352
R (Å)	4.4
D (Å)	0.840 189
α_{www}	0.0
b_f (Å^{-1})	12
r_f (Å)	1.3

$$f^c(r) = \begin{cases} 1, & r \le R - D, \\ \frac{1}{2} - \frac{1}{2}\sin\left[\frac{\pi}{2}(r-R)/D\right], & |R-r| \le D, \\ 0, & r \ge R + D, \end{cases}$$

where D and R are adjustable quantities. The bond-order parameter $b_{ij}=(1+\chi_{ij})^{-1/2}$ includes three-body contributions and angular dependence

$$\chi_{ij} = \sum_{k(\neq i,j)} f_{ik}^c(r_{ik}) g_{ik}(\theta_{ijk}) \times \exp[\alpha_{ijk}(r_{ij} - r_{ik})].$$

Here again the cutoff-function is included, while the indices monitor the atom type-dependence of the parameters, which is of importance for the description of compounds. α_{ijk} is a fitting parameter. The angular function is defined as follows:

$$g(\theta) = \gamma\left[1 + \frac{c^2}{d^2} - \frac{c^2}{d^2 + (h + \cos\,\theta)^2}\right],$$

where γ, c, d, and h are fitting parameters. In simulations with high-energy collisions ($E_{\mathrm{kin}} \gg 10$ eV), the repulsive part of the potential has to be modified as follows:

$$V_{\mathrm{mod}}^{\mathrm{R}}(r) = V^{\mathrm{PP}}(r)[1 - F(r)] + V^{\mathrm{R}}(r)F(r),$$

where V^{PP} is a repulsive pair potential for a dimer employing a DFT method[20] or the Ziegler–Biersack–Littmark universal repulsive potential[21] and $F(r)$ is the Fermi function

$$F(r) = \frac{1}{1 + \exp[-b_f(r - r_f)]},$$

where the constants b_f and r_f are chosen such that the potential is effectively unmodified at the equilibrium and longer bonding distances, but also gives smooth fit to the repulsive potential. The potential parameters, see Table I, were obtained by fitting simultaneously the cohesion energies and lattice constants of α and β phase W, elastic constants and bulk modulus, monovacancy formation and migration energies, and self-interstitial atom configuration and formation energy. The optimization algorithm used was the multidimensional unconstrained nonlinear Nelder–Mead method.[22]

III. TOTAL ENERGY CALCULATIONS

The DFT calculations were performed with the VASP.[23,24] The electronic ground state of the system was calculated using the projector-augmented wave[25,26] potentials as provided in VASP. Electron exchange-correlation was performed within the generalized gradient approximation using Perdew–Burke–Ernzerhof functionals.[27,28] The conjugate gradient algorithm[29] was used for the volumetric and ionic relaxation and the relaxation was stopped after a convergence criteria of 0.01 eV/Å was reached. The energy cutoff for calculations was 450 eV which ensured the convergence of geometrical structures and total energies. A supercell with periodic boundary conditions was used with 127 and 251 atoms for vacancy and interstitial systems, respectively. A more detailed description can be found elsewhere.[30]

IV. BULK PROPERTIES

Any potential model should be thoroughly tested by comparing different calculated properties and energies to experimental values. If experimental data are not available, the comparison should be made to DFT calculations. Before looking at point defects and thermal properties, it should be demonstrated that the potential gives the tungsten bulk properties satisfactorily. In Table II are presented the properties of various existing as well as hypothetical high symmetry bulk phases of tungsten as obtained from experiment, DFT calculations, other existing analytical potentials, and present BOP. The cohesion energy and lattice constant are close to the experimental ones for every potential, with the body-centered cubic (bcc) structure (α-W) as the most stable structure for tungsten. The experimentally observed lattice constants[33] of β-W and γ-W and the cohesive energies from DFT are nicely reproduced by our BOP. Even though the bulk modulus and elastic constants were taken into fitting, it was not possible to find a potential parameter set giving both the elastic constants and the point defect properties accurately (see Table III). Because the point defect concentrations and mobilities are exponential functions of formation and migration energies, they were considered more important than the elastic constants in the fitting procedure.

V. THERMAL AND POINT DEFECT PROPERTIES

To understand the changes in the microstructure and mechanical properties of a material during thermal treatment or irradiation, one has to have a definite picture of the kinetics and energetics of point defects. Table III summarizes the thermal and point defect properties obtained from experiment, DFT calculations, and analytical potentials. A large scatter in the melting temperature for the different analytical potentials is observed. The developed BOP overestimates the melting temperature by about 23%. Melting of the material is a complicated process, but a general observation can be stated as follows. If the formation energy for a Frenkel pair (sum of vacancy and interstitial formation energies: $H_v^f + H_i^f$) given by a potential is larger than the experimental one, the melting temperature calculated with the potential will also be larger than the one obtained experimentally.

TABLE II. Comparison of properties of the existing as well as the hypothetical high symmetry bulk phases of tungsten as obtained from experiment, DFT calculations, the FS potential, modified (MEAM) potential, and BOP by Mrovec *et al.* (Ref. 32), Juslin *et al.*(Ref. 14), and from the present study. E_c: cohesive energy (eV/atom); ΔE: energy difference with respect to ground-state structure (eV/atom); a: lattice parameter (Å); B: bulk modulus (GPa); and c_{ij}: elastic constants (GPa).

					Bond order potentials		
	Experimental	DFT	FS[a]	MEAM[b]	Mrovec *et al.*[c]	Juslin *et al.*[a]	Present study
Diamond							
ΔE		2.33[a]	3.11	3.70		3.11	4.46
a		5.87[a]	5.87	5.66		5.94	6.01
sc							
ΔE		1.35[c]	1.50	2.61	1.23	1.61	2.07
a		2.61[c]	2.69	2.63	2.52	2.67	2.59
hcp							
ΔE		0.47[c]				0.34	0.25
fcc, γ-W							
ΔE		0.47[c], 0.49[d]	0.15	0.26	0.48	0.35	0.24
a	4.13[e]	4.00[c], 4.02[d]	3.93	4.01	4.02	4.01	4.05
A15, β-W							
ΔE		0.08[c], 0.09[d]	0.22		0.64	0.31	0.10[e]
a	5.05[f]	5.06[c], 5.06[d]	5.14		5.07	5.12	5.16
bcc, α-W							
E_c	−8.9[f]	−9.97[g], −8.49[d]	−8.89	−8.66	−8.99	−8.89	−8.89[e]
a	3.165[i]	3.14[g], 3.172[d]	3.165	3.164	3.165	3.165	3.171[e]
B	308–314[h]	320[i]	301	314		308	215[e]
c_{11}	501–521[h]	552[i]	512	533		542	444[e]
c_{12}	199–207[h]	204[i]	196	205		191	128[e]
c_{44}	151–160[h]	149[i]	170	163		162	134[e]

[a]Reference 14.
[b]Reference 31.
[c]Reference 32.
[d]This work.
[e]Properties used in potential fitting.
[f]Reference 33.
[g]Reference 34.
[h]Reference 35.
[i]Reference 36.

A. Monovacancy

The vacancy formation energy of 3.75 eV calculated with our BOP is very close to the experimental value, and the vacancy formation volume agrees with DFT calculations. The FS type potential by Derlet *et al.*[13] gives also a nice formation value of 3.56 eV. The BOP by Juslin *et al.*[14] gives a quite low formation energy of 1.68 eV, while the BOP by Mrovec *et al.*[32] gives a bit high vacancy formation energy of 4.30 eV.

The W self-diffusion activation enthalpy of about 5.4 eV is the sum of vacancy formation and migration energies at temperatures where only monovacancy contributes to diffusion.[42] Both the experiments and BOP result in a monovacancy migration energy close to 1.8 eV. Moreover, the monovacancy migration barrier as a function of the reaction coordinate is in excellent agreement with DFT calculations (see Fig. 1). A positive migration volume of about 0.13 Ω estimated by our BOP predicts only a minor decrease in the monovacancy diffusivity at increasing pressures.[43]

B. Self-interstitial atom

The formation energy of SIA given by our BOP is in reasonable agreement with the experimental and DFT values. Study by Nguyen-Manh *et al.*[37] shows that ⟨111⟩ crowdion is the lowest energy SIA configuration for all nonmagnetic 5B and 6B transition metals. This SIA configuration agrees nicely with our DFT calculations and BOP (see Fig. 2). The small SIA formation volume of 0.6 Ω given by DFT is probably a consequence of the small system size (251 atoms) compared to the large SIA defect and periodic boundary conditions employed in the calculations.

The SIA configuration in W has a large extent in the lattice and its strain field reaches far from the SIA center. Figure 3 shows the SIA-monovacancy recombination radius around the ⟨111⟩ SIA crowdion calculated by the present BOP. If a monovacancy is inside the drawn ellipsoid, the Frenkel pair is annihilated.

The recombination radius is here defined as the maximum distance between the monovacancy and SIA center which allows immediate recombination and leaves behind a

TABLE III. Comparison of thermal and point defect properties obtained from experiment, DFT calculations, MEAM potential, BOP by Juslin *et al.*, and present study. T_m: melting temperature (K); ΔH_f: enthalpy of fusion at the melting temperature (kJ/mole); $\Delta V/V_s$: volume change upon melting (%); ρ_l: density of the liquid at the melting point (g/cm^3); α_L: coefficient of linear thermal expansion (10^{-6}/K); H_v^f, H_i^f: vacancy and interstitial formation energies (eV); V_v^f, V_i^f: vacancy and interstitial formation volumes in units of the atomic volume (Ω); H_v^m, H_i^m: vacancy and interstitial migration energies (eV); and V_v^m: vacancy migration volume (Ω).

		DFT			BOP	
	Experimental	Nguyen-Manh[a]	This work	MEAM[b]	Juslin *et al.*[c]	Present study
T_m	3695[d]			4600	2750	4550
ΔH_f	52.3[d]			33.0	27.4	31.8
$\Delta V/V_s$				3.2	4.3	3.6
ρ_l	17.0[d]				17.1	16.8
α_L	4.5[e]				6.6	8.2
H_v^f	3.7 ± 0.2 [f]	3.56	3.34	3.95	1.68	3.75[g]
V_v^f			0.62		0.68	0.73
H_v^m	1.8 ± 0.1 [f]	1.78	1.71		1.73	1.80[g]
V_v^m					−0.05	0.13
H_i^f	9.1 ± 0.6 [h]	9.6	9.98	9.0	8.3	9.9[g]
V_i^f			0.6		1.95	1.60
H_i^m		0.05	0.005		0.20	0.002

[a]Reference 37.
[b]Reference 31.
[c]Reference 14.
[d]Reference 38.
[e]Reference 39.
[f]Reference 40.
[g]Properties used in potential fitting.
[h]Reference 41.

perfect lattice. According to our calculations, the oblong shape of the SIA defect in W results in that the recombination radius is an ellipse (ellipsoid in three-dimensional) with the semiminor axis of 5.4 Å and semimajor axis of 18 Å. The recombination radius was calculated by placing a monovacancy in all positions around the SIA and relaxing each different system with the molecular statics method. The calculations were done using 5488 atoms but only the closest atoms in the crowdion plane are pictured in Fig. 3.

Under irradiation, an important factor driving the evolution of the microstructure in metals is the fast migration of SIA's. The crowdion configuration of the SIA in W, see Fig. 2, means that with only a small coherent displacement (~0.4 Å) of the crowdion atoms, the SIA center moves about 2.7 Å in ⟨111⟩ direction. This kind of behavior can be described by the Frenkel–Kontorova model which approximates the interstitial crowdion as a string of atoms connected by elastic springs.[44,45] As a result the interstitial crowdion can be described as a quasiparticle which can propagate through the crystal as a nearly free particle with an effective mass of only a fraction of that for a W atom. It follows that an interstitial crowdion should be very mobile along the crowdion axis, which is exactly what is observed. Dausinger *et al.*[46] concluded from their resistivity annealing experiments that long-range SIA migration starts between 24 and 30 K, corresponding to a migration energy of 54 meV. More resent work by Tamimoto *et al.*[47] using anelasticity measurements, indicates that SIA diffusion could already take place

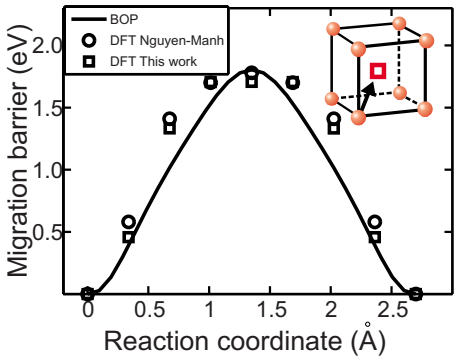

FIG. 1. (Color online) System energy variation along monovacancy migration path in ⟨111⟩ direction calculated by BOP and DFT methods. The saddle point energy is about 1.8 eV.

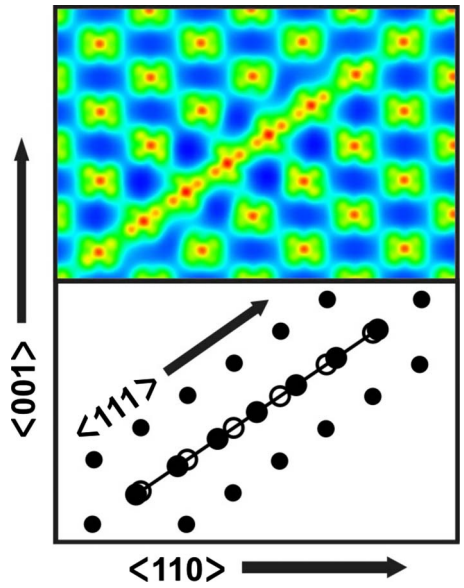

FIG. 2. (Color online) Top: electron density for the ⟨111⟩ crowdion calculated by DFT in this work. Bottom: the SIA configuration with the lowest energy for BOP developed in this study. The SIA displaces atoms (full circles) from their lattice sites (empty circles) in the ⟨111⟩ direction.

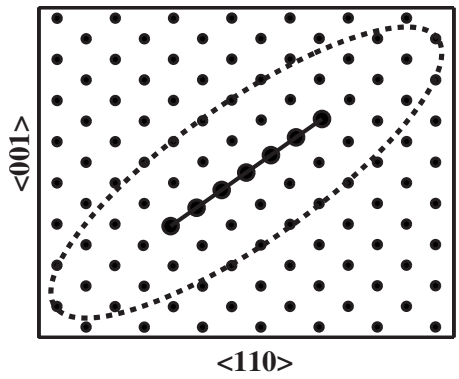

FIG. 3. The oblong shape of the SIA defect in W results in that the recombination radius is an ellipsoid around the center of the SIA with the semimajor axis 18 Å in ⟨111⟩ direction and semiminor axis 5.4 Å. If a SIA comes within this recombination radius from the monovacancy, they both are annihilated.

under 1.5 K. This low migration temperature would correspond to a much lower migration energy than 54 meV, as was obtained by our DFT calculations using 251 atoms with the nudged elastic band method. The SIA migration barrier calculated by DFT was 5 meV and by our BOP 2 meV.

VI. EXTENDED DEFECTS

In this section, we will first use the present BOP parameters set to look at the surface energies and interlayer relaxations for the low-index W surfaces. Second we will use the potential to calculate the configuration, trapping radius, and binding energies for W vacancy clusters.

A. Surfaces

The surface energy defined as the excess energy per surface unit area is an important quantity which determines for example the equilibrium shape of the mesoscopic crystals. The surface energies and interlayer relaxations for the unreconstructed low-index surfaces (100), (110), (111), and (211) are presented in Table IV. The experimental surface energy values of 3.27 and 3.68 J/m^2 results from surface tension measurements in the liquid phase extrapolated to zero temperature.[48,49] Thus, these values correspond to an isotropic crystal and cannot be compared with the surface energy of a particular surface facet. The surface energies for the present BOP seem to be slightly smaller than for the BOP by Mrovec *et al.*[32] or given by DFT calculations. The interlayer relaxations, however, are in agreement with the existing experimental and DFT values.

B. Vacancy clusters

As the thermal energy increases, the monovacancies start to diffuse. If the moving vacancy comes into contact with another vacancy or vacancy cluster, and the interaction is attractive, the vacancy is trapped and a bigger cluster is formed. Table V shows the binding energies for small vacancy clusters obtained in this study. The corresponding configurations for the vacancy clusters can be seen in Fig. 4.

The binding energy of a vacancy cluster with N vacancies, E_N^b, is defined as the energy required to separate the last vacancy from the cluster as

TABLE IV. Surface energies and interlayer relaxations (%) for unreconstructed low-index surfaces obtained from experiment, DFT calculations and analytical potentials. γ^{hkl}: surface energy (J/m^2) for (hkl) surface; and Δ_{ij}^{hkl}: interlayer relaxation (%) between layer i and j.

				BOP	
	Expt.	DFT	FS[a]	Mrovec *et al.*[a]	This study
(100)					
γ^{100}		4.64[b]	2.92	3.81	2.91
Δ_{12}^{100}	−6[c], −4 ± 10 [d]	−6 ± 0.5 [e]	−0.7	−2.5	−2.3
Δ_{23}^{100}		0.5 ± 0.5 [e]	−0.6	−0.4	−1.8
(110)					
γ^{110}		4.01[b]	2.58	2.60	2.17
Δ_{12}^{110}	−2.7 ± 0.5 [f]	−3.6[g]	−0.5	−1.0	−3.3
Δ_{23}^{110}	0.0 ± 0.3 [f]	+0.2 [g]	+0.1	+0.6	+0.2
(211)					
γ^{211}		4.18[b]	3.05	3.00	2.80
Δ_{12}^{211}	−9.3[h]		−4.8	−7.9	−8.6
Δ_{23}^{211}			+1.1	+2.1	−1.3
(111)					
γ^{111}		4.45[b]			3.24
Δ_{12}^{111}					−5.7
Δ_{23}^{111}					−16.4

[a]Reference 32.
[b]Reference 50.
[c]Reference 51.
[d]Reference 52.
[e]Reference 53.
[f]Reference 54.
[g]Reference 55.
[h]Reference 56.

TABLE V. Binding energies for small vacancy clusters. The binding energy is defined as the energy required to separate the last vacancy from the cluster.

Number of vacancy in the cluster	Binding energy (eV)	Number of vacancy in the cluster	Binding energy (eV)
2[a]	0.6559	7	1.7459
3	1.1127	8	1.8353
4	1.8942	9	2.2658
5	1.7833	10	2.2686
6	2.2953		

[a]Nearest neighbor configuration

$$E_N^b = E_{N-1} + E_1 - (E_N + E_0),$$

where E_N is the total energy of the system. To perform the calculation, one needs to find the lowest potential energy configuration for each cluster size. In this work, this was done by using a simulation cell with 5488 lattice positions and the system total potential energy for each possible vacancy configuration was calculated using molecular statics method. The nearest neighbor divacancy binding energy obtained by present BOP was 0.66 eV, which is very close to the only existing experimental value of 0.7 eV by Park *et al.*[57] There is some controversy whether the binding energy of the divacancy is positive or negative; DFT values vary between −0.4 and +1.0 eV, as discussed in Ref. 58 and references therein.

Finding the lowest energy configuration for large vacancy clusters can be very time consuming computationally. For example, four vacancies can be distributed in 10 different lattice positions in 210 different ways. The number of different possible configurations N_{Conf} that N_{Vac} number of vacancies can be arranged in N_{Pos} lattice positions can be calculated using the equation

$$N_{Conf} = \frac{N_{Pos}(N_{Pos}-1)\ldots(N_{Pos}-N_{Vac}+1)}{N_{Vac}}.$$

As can be noticed, the number of possible vacancy configurations increases very fast for larger clusters; 10 vacancies can be distributed in 24 different lattice positions in 196 1256 different ways. An approach to decrease the computational effort in finding the lowest energy configuration is the use of the fact that W atoms in a bcc lattice have eight nearest neighbors at a distance of about 2.74 Å. If any of the eight nearest atoms are missing for a particular W atom, the calculated total potential energy increases. The minimum energy configuration for a vacancy cluster should thus be a configuration where the total number of nearest neighbors in the lattice is at its maximum. Total energy calculations are thus needed only for those cluster configurations that result in a small number of broken W bonds, reducing drastically the computational effort in finding the lowest vacancy cluster configuration.

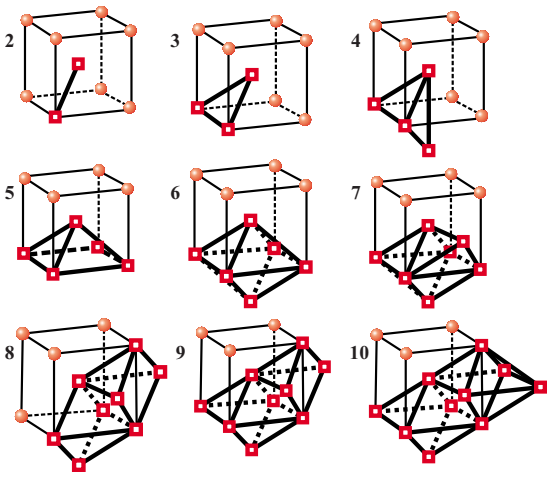

FIG. 4. (Color online) Lowest energy configurations for small vacancy clusters calculated using the present BOP. We can see that square pyramid (five vacancies) shapes are favored, leading also to octahedral shapes (six vacancies) which also is a square bipyramid.

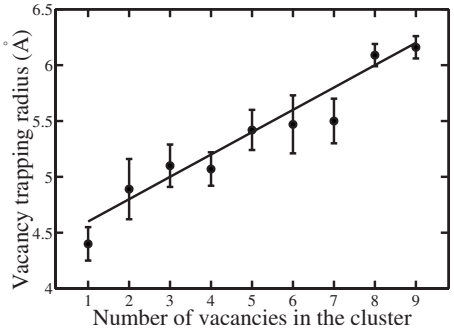

FIG. 5. The vacancy trapping radius increases approximately linearly with the size of the vacancy cluster. If a monovacancy comes within this distance from the vacancy cluster center, it will be trapped and the cluster size will increase by 1.

Next, the present BOP parameters were used to calculate the distance of a monovacancy to a vacancy cluster before it is trapped and the cluster size increases by 1. This parameter, called the vacancy trapping radius R_T^v, is measured from the cluster center. The resulting vacancy trapping radius as a function of cluster size calculated using molecular statics is presented in Fig. 5. The vacancy trapping radius increases approximately linearly with the size of the cluster N_{Vac} and is fitted by a straight line

$$R_T^v = (4.4 + 0.2N_{Vac}) \text{ Å}.$$

The nonspherical configurations for small vacancy clusters are responsible for the linear increase in the trapping radius. The larger the vacancy clusters become, the more spherical they appear. For large clusters the vacancy trapping radius should increase proportional to $N_{Vac}^{1/3}$.

VII. CONCLUSIONS

A set of parameters for a reactive interatomic bond-order potential giving accurate formation and migration energies for point defects in tungsten and able to deal with high-energy collisions was presented. The obtained potential parameters set was used to calculate various properties in W, including the binding energies and trapping distances for vacancies in vacancy clusters and the recombination radius for the self-interstitial atom and monovacancy.

ACKNOWLEDGMENTS

The research was supported by Association EURATOM-TEKES under the FUSION program. Grants of computer time from the Center for Scientific Computing (CSC) in Espoo, Finland are gratefully acknowledged.

[1]ITER Physics Basis Editors, ITER Physics Expert Group Chairs and Co-Chairs, and ITER Joint Central Team and Physics Integration Unit, Nucl. Fusion **39**, 2137 (1999).
[2]A. T. Peacock, J. Nucl. Mater. **329–333**, 173 (2004).
[3]J. Friedel, *Dislocations* (Pergamon, Oxford, 1964).
[4]W. Schilling and K. Sonnenberg, J. Phys. F: Met. Phys. **3**, 322 (1973).
[5]J. W. Corbett, R. B. Smith, and R. M. Walker, Phys. Rev. **114**, 1452 (1959).
[6]S. Yip, *Handbook of Materials Modeling* (Springer, New York, 2005).
[7]M. S. Daw and M. I. Baskes, Phys. Rev. Lett. **50**, 1285 (1983).
[8]M. S. Daw and M. I. Baskes, Phys. Rev. B **29**, 6443 (1984).
[9]M. W. Finnis and J. E. Sinclair, Philos. Mag. A **50**, 45 (1984).
[10]M. I. Baskes, Phys. Rev. B **46**, 2727 (1992).
[11]*Tight-Binding Approach to Computational Materials Science*, edited by P. E. A. Turchi, A. Gonis, and L. Colombo (Materials Research Society, Pittsburg, 1998), Vol. 491.
[12]W. Xu and J. B. Adams, Surf. Sci. **301**, 371 (1994) and references therein.
[13]P. M. Derlet, D. Nguyen-Manh, and S. L. Dudarev, Phys. Rev. B **76**, 054107 (2007).
[14]N. Juslin, P. Erhart, P. Träskelin, J. Nord, K. O. E. Henriksson, E. Salonen, K. Nordlund, and K. Albe, J. Appl. Phys. **98**, 123520 (2005).
[15]J. Tersoff, Phys. Rev. Lett. **61**, 2879 (1988).
[16]D. W. Brenner, Phys. Rev. B **42**, 9458 (1990); **46**, 1948 (1992).
[17]D. W. Brenner, O. A. Shenderova, J. A. Harrison, S. J. Stuart, and S. B. Sinnott, J. Phys.: Condens. Matter **14**, 783 (2002).
[18]K. A. Albe, K. Nordlund, and R. S. Averback, Phys. Rev. B **65**, 195124 (2002).
[19]K. Albe, K. Nordlund, J. Nord, and A. Kuronen, Phys. Rev. B **66**, 035205 (2002).
[20]K. Nordlund, N. Runeberg, and D. Sundholm, Nucl. Instrum. Methods. Phys. Res. B **132**, 45 (1997).
[21]J. F. Ziegler, J. P. Biersack, and U. Littmark, *The Stopping and Range of Ions in Matter* (Pergamon, New York, 1985).
[22]N. Nelder and R. Mead, Comput. J. **7**, 308 (1965).
[23]G. Kresse and J. Hafner, Phys. Rev. B **47**, 558 (1993); **49**, 14251 (1994).
[24]G. Kresse and J. Furthmüller, Phys. Rev. B **54**, 11169 (1996).
[25]P. E. Blöchl, Phys. Rev. B **50**, 17953 (1994).
[26]G. Kresse and D. Joubert, Phys. Rev. B **59**, 1758 (1999).
[27]J. P. Perdew, K. Burke, and M. Ernzerhof, Phys. Rev. Lett. **77**, 3865 (1996).
[28]Y. Zhang and W. Yang, Phys. Rev. Lett. **80**, 890 (1998).
[29]W. H. Press, B. P. Flannery, and S. A. Teukolsky, *Numerical Recipes: The Art of Scientific Computing* (University Press, Cambridge, 1986).
[30]K. Heinola and T. Ahlgren, J. Appl. Phys. (submitted).
[31]B.-J. Lee, M. I. Baskes, H. Kim, and Y. K. Cho, Phys. Rev. B **64**, 184102 (2001).
[32]M. Mrovec, R. Gröger, A. G. Bailey, D. Nguyen-Manh, C. Elsässer, and V. Vitek, Phys. Rev. B **75**, 104119 (2007).
[33]E. Lassner and W.-D. Schubert, *Tungsten, Properties, Chemistry, Technology of the Element, Alloys, and Chemical Compounds* (Kluwer, Academic, Plenum Publishers, New York, 1999).
[34]T. Ochs, O. Beck, C. Elsasser, and B. Meyer, Philos. Mag. A **80**, 351 (2000).
[35]D. I. Bolef and J. de Klerk, J. Appl. Phys. **33**, 2311 (1962).
[36]K. Einarsdotter, B. Sadigh, G. Grimvall, and V. Ozolins, Phys. Rev. Lett. **79**, 2073 (1997).
[37]D. Nguyen-Manh, A. P. Horsfield, and S. L. Dudarev, Phys. Rev. B **73**, 020101 (2006).
[38]*CRC Handbook of Chemistry and Physics*, 85th ed., edited by D. R. Lide (CRC, Boca Raton, 2004).
[39]H. O. Pierson, *Handbook of Refractory Carbides and Nitrides* (Noyes, Westwood, NJ, 1996).
[40]K.-D. Rasch, R. W. Siegel, and H. Schultz, Philos. Mag. A **41**, 91 (1980).
[41]I. M. Neklyudov, E. V. Sadanov, G. D. Tolstolutskaja, V. A. Ksenofontov, T. I. Mazilova, and I. M. Mikhailovskij, Phys. Rev. B **78**, 115418 (2008).
[42]J. N. Mundy, S. J. Rothman, N. Q. Lam, H. A. Hoff, and L. J. Nowicki, Phys. Rev. B **18**, 6566 (1978).
[43]R. N. Jeffery and D. Lazarus, J. Appl. Phys. **41**, 3186 (1970).
[44]S. L. Dudarev, Philos. Mag. **83**, 3577 (2003).
[45]O. M. Braun and Y. S. Kivshar, Phys. Rep. **306**, 1 (1998).
[46]F. Dausinger and H. Schultz, Phys. Rev. Lett. **35**, 1773 (1975).
[47]H. Tamimoto, H. Mizubayashi, and S. Okuda, J. Phys. IV **6**, 285 (1996).
[48]W. R. Tyson and W. A. Miller, Surf. Sci. **62**, 267 (1977).
[49]F. R. de Boer, R. Boom, W. C. M. Mattens, A. R. Miedema, and A. K. Niessen, *Cohesion in Metals* (North-Holland, Amsterdam, 1988).
[50]L. Vitos, A. V. Ruban, H. L. Skriver, and J. Kollár, Surf. Sci. **411**, 186 (1998).
[51]C. L. Fu and A. J. Freeman, Phys. Rev. B **37**, 2685 (1988).
[52]M. S. Altman, P. J. Estrup, and I. K. Robinson, Phys. Rev. B **38**, 5211 (1988).
[53]R. Yu, H. Krakauer, and D. Singh, Phys. Rev. B **45**, 8671 (1992).
[54]H. L. Meyerheim, D. Sander, R. Popescu, P. Steadman, S. Ferrer, and J. Kirschner, Surf. Sci. **475**, 103 (2001).
[55]M. Arnold, G. Hupfauer, P. Bayer, L. Hammer, K. Heinz, B. Kohler, and M. Scheffler, Surf. Sci. **382**, 288 (1997).
[56]O. Grizzi, M. Shi, H. Bu, J. W. Rabalais, and P. Hochmann, Phys. Rev. B **40**, 10127 (1989).
[57]J. Y. Park, H.-C. W. Huang, R. W. Siegel, and R. W. Balluffi, Philos. Mag. A **48**, 397 (1983).
[58]C. S. Becquart and C. Domain, Nucl. Instrum Methods Phys. Res. B **255**, 23 (2007).